

The Effects of Atmospheric Turbulence on Simulated Starlight in a Low-Pressure Telescope Environment

Renee Park

under the direction of
Dr. Benjamin Lane
Massachusetts Institute of Technology

Research Science Institute
July 31, 2007

Abstract

We investigated the feasibility of using nulling interferometry techniques in the stratosphere to search for extra-solar planets. Studies have shown wavefront distortions from atmospheric turbulence to be too large to obtain clear ground-based images. Wavefront errors caused by atmospheric turbulence in the stratosphere are on the scale of 1 angstrom [4], however, the level of the wavefront error inside a telescope tube is unknown. We used Kite, a system level testbed created by the Jet Propulsion Laboratory for the External Metrology System of the Space Interferometry Mission, to simulate atmospheric turbulence conditions inside a telescope tube in the stratosphere. We obtained 40 minutes of laser metrology gauge readings in relatively stabilized temperatures at 5 mb. The data was analyzed using adaptive optics and blanking techniques to reduce the level of instrument noise. The integrated total error was approximately 1.849 angstroms, validating the possibility of applying nulling interferometry techniques without sending a telescope into space.

1 Introduction

The first extra-solar giant planet, 51 Pegasi b, was discovered in 1995 using Doppler spectroscopy [7]. Since then, scientists have endeavored to directly detect the presence of planets outside our solar system. However the small angular separation and high brightness contrast characteristic of star-planet systems has, thus far, prevented the use of direct detection of light from extra-solar planets. From 10 pc away, the planets from Mercury to Saturn are within 1" from the Sun. For these planets, the Sun-to-planet contrast ratio (the intensity of starlight versus the intensity of the light from a planet) exceeds 10^9 . While the angular separation cannot be adjusted, it is possible to lower the contrast ratio by observing in infrared, where the contrast ratio is smaller (10^3 to 10^6), or by finding a way to cancel the brightness of the star's light relative to its surroundings.

We are primarily interested in the optical methods of detection to provide direct images of the planets. Two techniques have proven promising in selectively attenuating the direct starlight to provide views of planets: coronagraphy and nulling interferometry [10]. Coronagraphy suppresses starlight by physically blocking the light from the star from the telescope detector. The residual starlight forms an Airy pattern of diffraction (Figure 1) and the method is only useful beyond several Airy radii away from the star as the residual light exceeds the light from the planet (Figure 2). Therefore, coronagraphy will be effective only for the closest stars. Nulling interferometry uses destructive interference to cancel light directly from a star. The residual pattern created by a nulling interferometer falls off faster with angle than does the residual from a coronagraph. This allows one to detect planets close to the star, resulting in a significant increase in the number of observable targets and/or allows one to use a significantly smaller telescope (factor of two).

The basis of nulling interferometry involves sampling an incoming wavefront with two apertures (telescopes), and adjusting internal paths such that when their wavefronts are

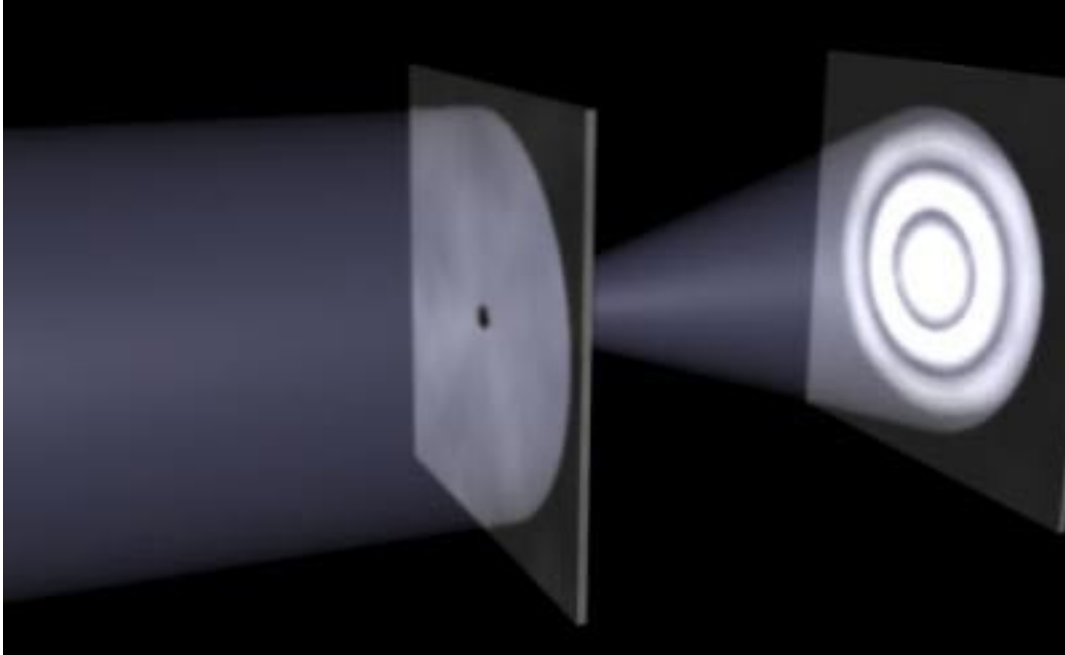


Figure 1: An Airy pattern forms when a light source passes through one hole. Nulling interferometry relies on two holes, forming a fringe pattern (a pattern of bars).[11]

combined, the two electric field vectors are exactly out of phase, causing them to cancel (Figure 3).

Until now, the use of nulling interferometry has been considered feasible only outside Earth's atmosphere, which is an expensive undertaking. Atmospheric turbulence distorts incoming light and is a major contributor to the difficulty of optical and infrared interferometry from the ground. Many of the key design parameters of an interferometer are driven largely by the boundary conditions set by the atmosphere [10]. However, researchers have recently proposed that nulling interferometry could be used by telescopes transported on balloons. Balloons are capable of taking an instrument to the stratosphere, higher than about 99.5% of the atmosphere and a slightly larger part of the atmospheric turbulence. Past research shows that the wavefront error caused by the remaining atmospheric turbulence is on the scale of 10^{-10} m [4]. The major open question regarding the use of a balloon is what level

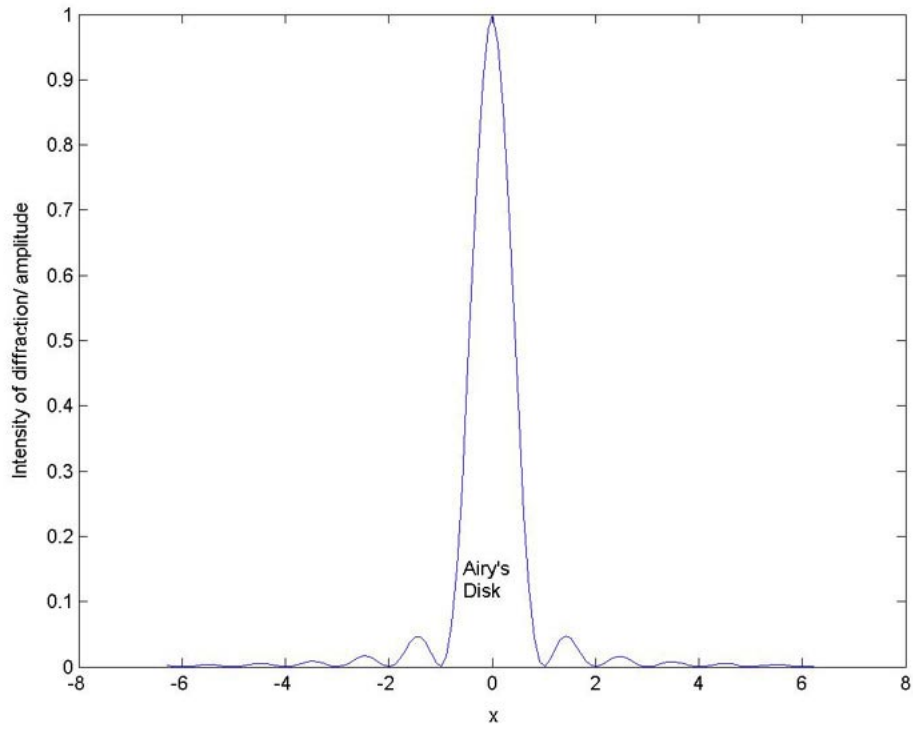


Figure 2: In an airy pattern, the intensity is higher closer towards the light source (almost like a side-view). According to the scale of this diagram, if a planet was within 1 unit from its star, the planet will not be visible even after using coronagraphy. [3]

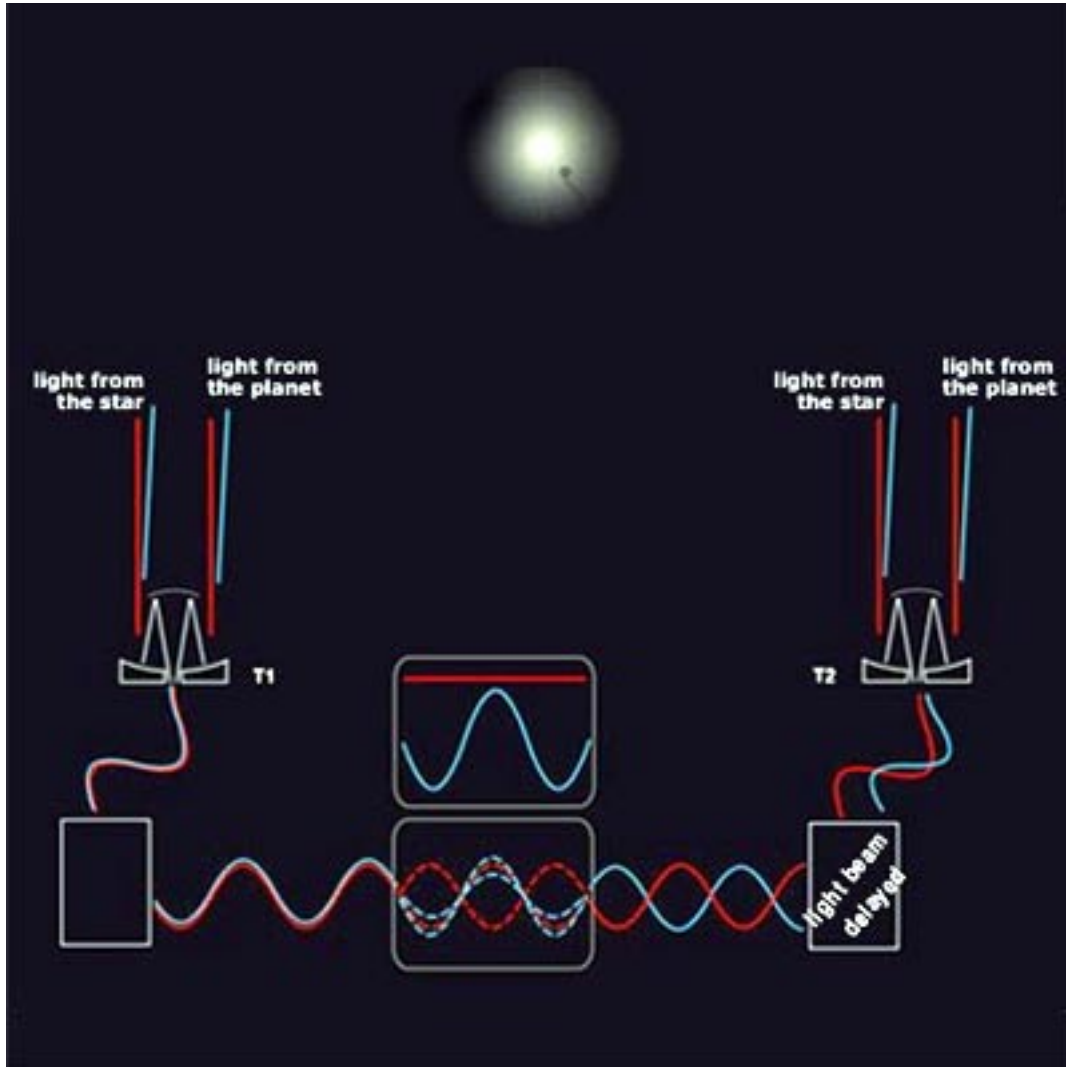


Figure 3: Nulling interferometry offsets two telescopes such that their images of a star cancel through destructive interference.[2]

of atmospheric turbulence is caused inside the telescope tube by the heat of the instrument at stratospheric altitudes.

To test the level of turbulence, we simulated conditions at the stratosphere using a vacuum chamber, and measured the residual optical turbulence.

If proven that nulling interferometry can be applied successfully from balloons, then these results will serve to validate wavefront control and nulling technology necessary for Terrestrial Planet Finder missions currently being proposed by NASA. This method could also be used to survey stars not yet viewed by other techniques or avoided for other difficulties with accuracy.

2 Materials and Methods

2.1 Experimental Design

Data was collected using Kite, a testbed designed by the Jet Propulsion Laboratory for the External Metrology System of NASA’s Space Interferometry Mission [1]. The original purpose of Kite was to test laser metrology gauges in simulated space conditions. Laser metrology gauges monitor internal and external optical path distances required for astrometric measurements, using beam launchers to direct a metrology beam at a target and collect the returning laser light. The gauges are used for high-bandwidth sensing of phasing errors. We used metrology gauges inside a vacuum chamber that was adjusted to a pressure level of 5 millibars (3.5 torr), similar to that of the Earth’s stratosphere.

Inside the chamber were six fiducials defining the baseline vectors and metrology gauges measuring the distances between the fiducials; the absolute lengths between the fiducials, on the order of 10 microns, are known as 1.571615, 2.983117, 1.477939, 1.457499, 0.534182, 1.551161 for L1 to L6, respectively [1]. Four of the fiducials were double corner cubes and the other two were triple corner cubes all made of retroreflecting mirrors as shown in Figure 4;

corner cubes are sets of mirrors arranged to reflect light from any direction directly back to its source. Kite measured the consistency between gauge measurements. Any path differences can be attributed to the remaining atmosphere, or electrical noise in the metrology gauges. However, the electrical noise tends to occur at specific frequencies and can thus be filtered out.

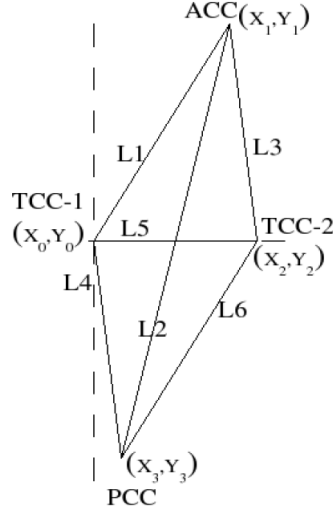


Figure 4: A schematic of the Kite instrument. Clockwise from left: triple corner cube 1 (TCC-1), articulating corner cube (ACC), triple corner cube 2 (TCC-2), and pointing corner cube (PCC). The “distances” between each pair of corners are labeled L1 to L6.[1]

2.2 Data Processing

2.2.1 Degree of Error

To evaluate the extent to which air turbulence effects traveling light waves, the predicted lengths measured by gauge 2 are calculated from the other five gauges and then compared to the actual readings from gauge 2. The points in Figure 4 $((x_0, y_0), (x_1, y_1), (x_2, y_2), (x_3, y_3))$ are placed on a coordinate plane where (x_0, y_0) is the origin and (x_2, y_2) is on the x-axis.

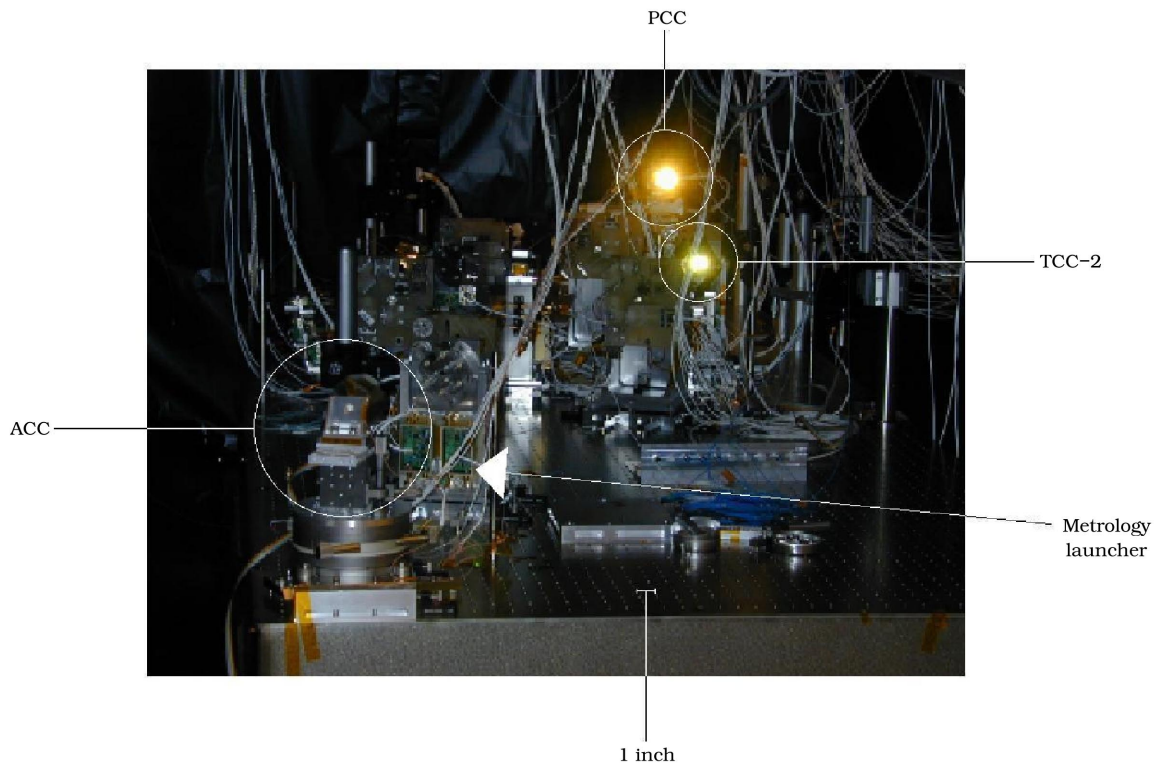


Figure 5: A photo of the Kite instrument. Note that the camera's flash is reflected directly back from the PCC and the TCC-2 because they are retroreflecting mirrors.[1]

The lengths are denoted l_i where i runs from 1 to 6. Subsequently, we have

$$(x_1, y_1) = \left(\frac{l_5^2 - l_1^2 + l_3^2}{2l_5}, -\sqrt{l_3^2 - x_1^2} \right) \quad (1)$$

$$(x_2, y_2) = (l_5, 0) \quad (2)$$

$$(x_3, y_3) = \left(\frac{l_5^2 - l_4^2 + l_6^2}{2l_5}, -\sqrt{l_6^2 - x_3^2} \right) \quad (3)$$

Thus, we find the predicted length between the top and bottom fiducials, whose actual length was read by gauge 2, can be expressed by the distance equation: $l'_2 = \sqrt{(x_1 - x_3)^2 + (y_1 - y_3)^2}$.

The residual, or the difference between the predicted and measured length, is

$$\Delta \equiv l_2 - l'_2 \quad (4)$$

Note, however, that for equations 1 through 4, the length is the absolute length, but the Kite instrument is only capable of measuring relative motions. Therefore, a control step called the “Absolute Metrology” mode determines the absolute length down to a resolution of tens of microns. Once the initial lengths have been determined, we add them to the relative gauge measurements before analyzing the data.

2.2.2 Power Spectral Analysis

We evaluate the magnitude of the gauge residual produced by atmospheric turbulence using power spectral densities (PSDs). PSDs are based on a method called Fourier transform, which takes wave readings and gives information about the frequencies in those readings. The transformation restates periodic data as the sum of various sine and cosine waves. Based on the Euler formulae

$$\cos \rho = \frac{e^{i\rho} + e^{-i\rho}}{2} \quad (5)$$

$$\sin \rho = \frac{e^{i\rho} - e^{-i\rho}}{2i} \quad (6)$$

we can use the Fourier integral in Octave, a freely distributed software based on Matlab that is primarily written for numerical computations, to obtain PSDs of the data. The integral is as follows

$$F(\omega) = \frac{1}{2\pi} \int_{-\infty}^{\infty} f(t) e^{2\pi i \omega t} dt \quad (7)$$

where $f(t)$ is a function of time and $F(\omega)$ is a function of wavelength.

2.2.3 Adaptive Optics

Once PSDs are obtained, the data must be corrected in a number of ways to reduce background noise. Because the Kite instrument uses adaptive optics, noise at low frequencies can typically be attributed to its servo system. A servo system is an optical system that adapts to compensate for optical effects introduced by the medium between, in this case, a star and a detector. The system, usually operating at frequencies of 10 to 1000 Hz, actively tracks and corrects observational changes in a path. A simple servo system operates on one output parameter and is affected by some external disturbance. In order to control the system such that the result is as close as possible to the desired input, the sensor reads the output and corrects the command accordingly in a “feedback” system. However, although a servo system does correct most of the error caused by observational changes in the path, it also introduces some instrumental error that can be subtracted.

We want to quantify the effect of adding a notional servo loop to correct for the low-frequency path-length changes observed in the Kite data. We can use basic first-order servo theory to derive the servo noise rejection factor as a function of frequency, which is:

$$\frac{1}{1 + \left(\frac{f_c}{f}\right)^2} \quad (8)$$

where f is the frequency and f_c is the constant closed loop frequency, or how fast the servo system can correct the response time error.

2.2.4 Blanking Peaks

In addition to using adaptive optics to correct the wavefront error, a blanking technique can be used to remove error caused by instrument vibrations. Raw data will show a combination of sinusoidal waves when there is instrumental noise; the data will look periodic, which cannot be caused by atmospheric turbulence since atmospheric changes are random. On a PSD plot, the exact frequencies of the sinusoidal waves are seen as large peaks which are then easily blanked by cutting off the peaks above a reasonable value and setting those frequencies to the average value of the entire plot. From previous experience, we expect instrumental noise to be at frequencies around 6 Hz and 10 Hz.

3 Results

We collected data using JPL's Kite instrument for over two hours. Since the temperature inside the vacuum did not stabilize while the pressure was being lowered, we only analyzed the final forty minutes of data (see Figure 6).

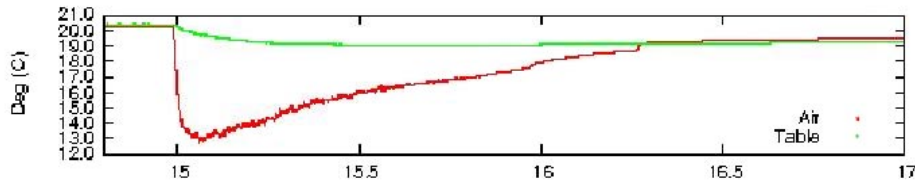


Figure 6: Temperature inside the vacuum chamber from 15 hours to 17 hours.

For clarity, we show the raw data detrended to one degree (Figure 7). The data has been decimated so that only one out of every hundred points are shown. No corner cubes are

articulating and the vibrations only reflect instrument noise. However, note that gauges 1 through 3 have much stronger vibrations than gauges 4 through 6 because the first three gauges each see the articulating corner cube, which is excited by vacuum tank modes causing about 50 nm vibrations.

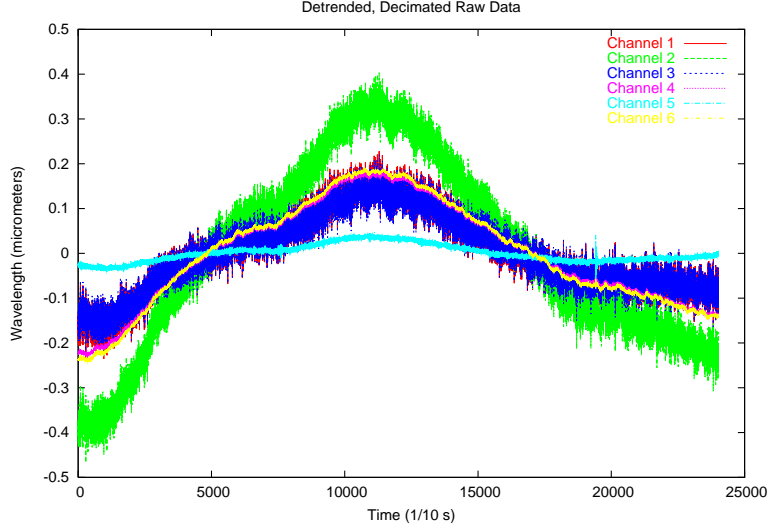


Figure 7: Detrended, raw, decimated data of all six channels.

The residual graph and the PSD of the residuals (Figures 8 and 9) both reflect a combination of sinusoidal functions affecting the data. As atmospheric turbulence is random, we know the periodic data is due to instrumental vibrations and can blank out their effects. By integrating the plots, illustrated by the cumulative sums on Figure 9, we know the total error is 1.264 nm and should be on the scale of a few angstroms after servo system corrections and blanking.

The servo system correction was applied with a calculated closed loop frequency of 0.02 Hz. The result can be seen in Figure 10 where the PSD shows a rapid drop in the values in the lower frequencies. The cumulative sum at this point was approximately 3.314 angstroms.

Figure 10 also shows the plot after both servo corrections and blankings were applied. The large peaks around 6 Hz and 10 Hz in Figure 8 were blanked out, lowering all values

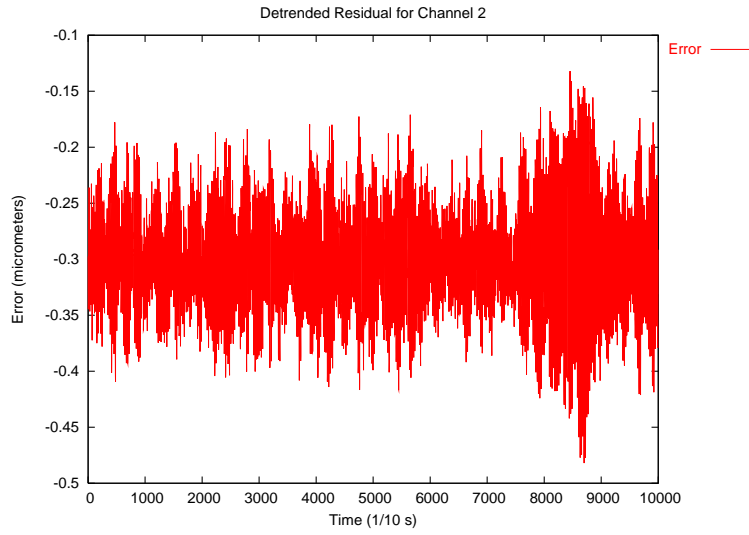


Figure 8: Detrended residual of first 10,000 points. Note the periodicities of the error.

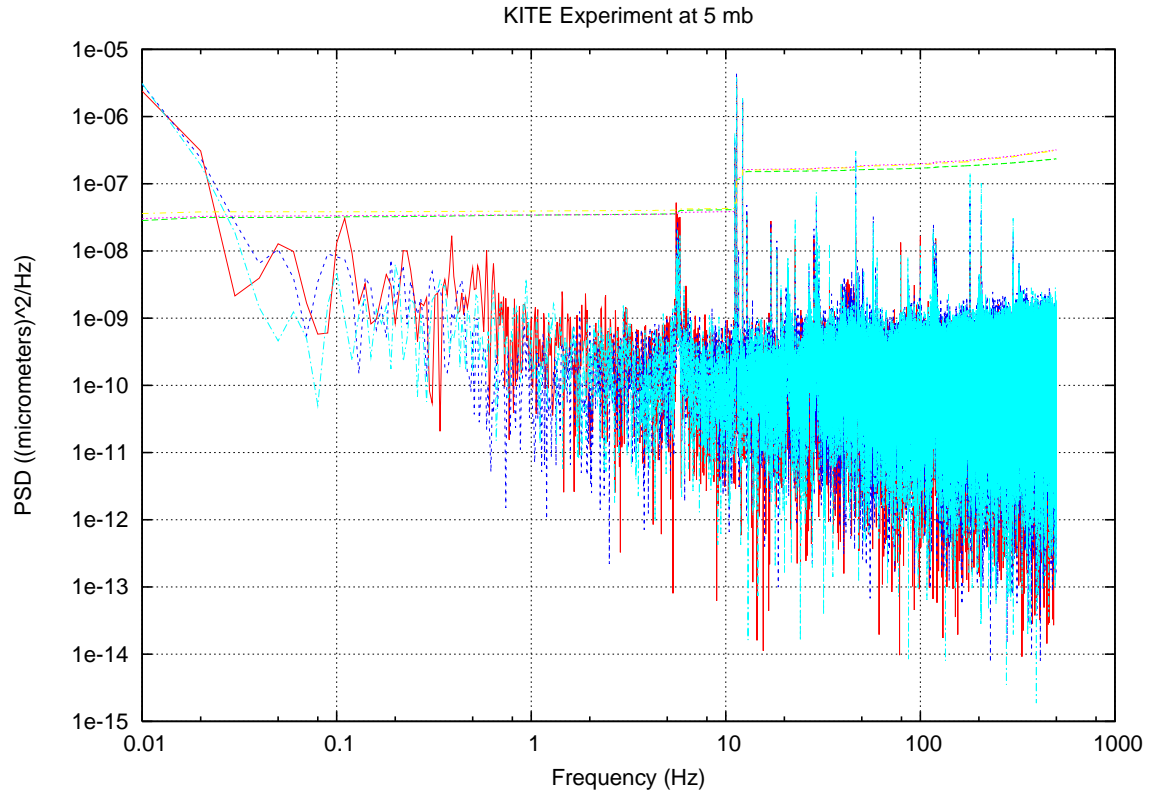


Figure 9: The PSD of three sets of 100,000 points from the residual and their cumulative sums.

above 10^{-8} to 10^{-10} for all frequencies greater than 1 Hz. The final cumulative error was 1.849 angstroms, which is a little less than twice the wavefront error found in the stratosphere [4]. Even beyond 10 Hz, the PSD shows large fluctuations. However, these points are random noise at low levels and do not amount to much integrated power.

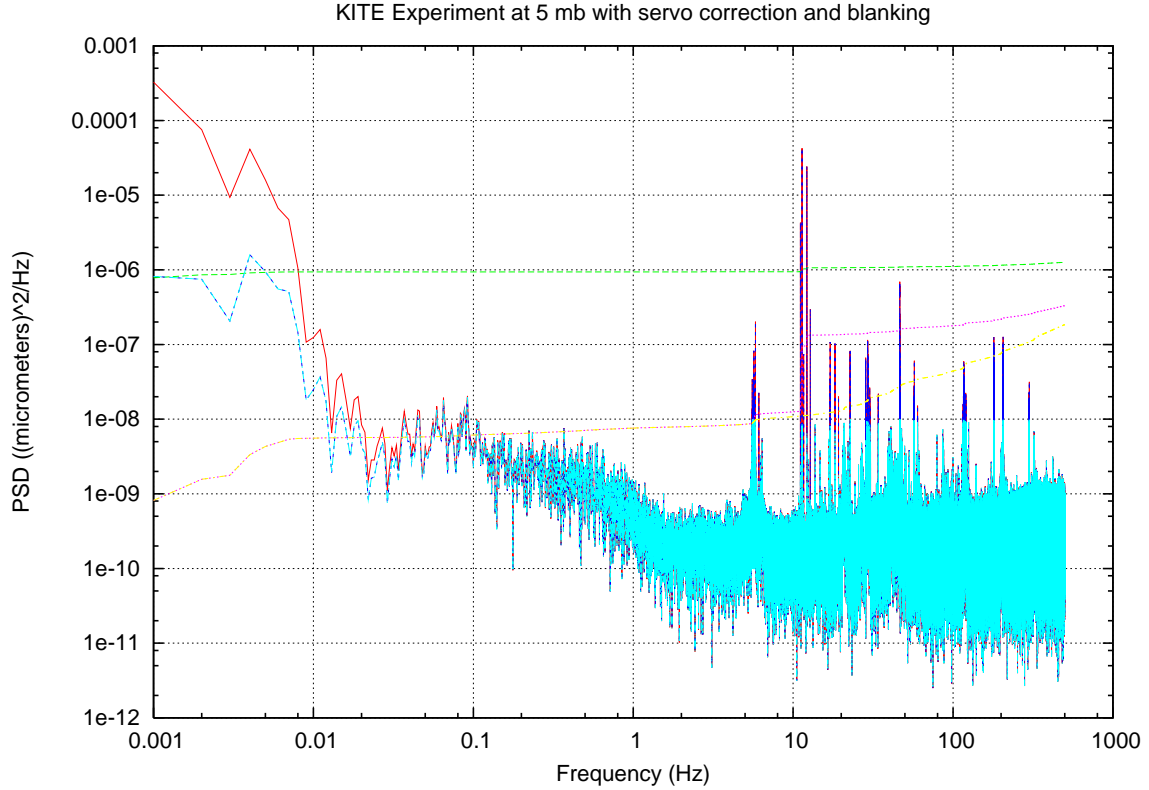


Figure 10: Three plots showing the original PSD (red), the PSD after the servo correction has been applied (dark blue), and the PSD after the servo correction and the blanking have been applied (light blue). Each plot is accompanied by their cumulative sums in green, pink, and yellow, respectively.

4 Conclusion

Using adaptive optics and blanking techniques, we have shown that in an environment approximating the conditions found in the stratosphere, the root mean square pathlength error

caused by turbulence over a path of 2.983 meters is 1.849 angstroms. We note also that the temperature difference between the air and the table was ± 0.1 degrees Celsius. The level of turbulence typically scales with Δt (temperature) to the power of 1.2. Blanking techniques, instead of filtering techniques, were used because although results would be more accurate with filtration, the difference in the respective results would be small enough to be insignificant.

Our results are very promising as the error from atmospheric turbulence is only one-fifth of a wavelength. When spread out over an image of 1000 pixels, the error per pixel is only 0.0002. This error is sufficiently small that it will not mask the intensity of a planet's light.

We hope to use this data to support the use of balloon-borne telescopes for gathering data on extra-solar planets. This venture could be completed in 3 to 4 years, whereas building another Hubble-like telescope will not be completed for at least another decade.

5 Acknowledgments

I would like to thank my mentor, Dr. Benjamin F. Lane of the Massachusetts Institute of Technology, for all his invaluable help and guidance in this project, the researchers at Caltech who ran our experiment on the Kite instrument, and his colleagues Professor Edmund Bertschinger and Dr. Miguel Morales for their instruction on background information. I would also like to thank Balint Veto, my tutor at the Research Science Institute, for his support and comments. Finally, I would like to thank the Center for Excellence in Education for providing me the chance to work on this project.

References

- [1] Dekens, Frank G., et al: *Kite: Status of the External Metrology Testbed for SIM*. Jet Propulsion Laboratory: California Institute of Technology, 2004.
- [2] European Space Agency. *ESA to test the smartest technique for detecting extra-solar planets from the ground* Available at http://www.esa.int/export/esaCP/ESAEQFF18ZC_Life_1.html (2004/07/19).
- [3] Glossary of PRIMA. *Airy's disk* Available at http://www.eso.org/projects/vlti/instru/prima/glossary_prima.html (2004/07/19).
- [4] Greenwood, D.P.: Bandwidth specifications for adaptive optics systems. *Journal of Optical Society of America*. **67** (1977): 390-2.
- [5] Lane, Benjamin: High Precision Infra-red Stellar Interferometry. *PhD thesis*, 2003.
- [6] Lane, Benjamin: Prospects of a Balloon-borne Planet Imager. *Proposal to NASA*, 19 April 2004.
- [7] Mayor, M., Queloz, D.: A Jupiter-Mass Companion to a Solar-Type Star. *Nature*. **378** (1995): 355.
- [8] Pallas, Lembit: *Harmonic Analysis*. Available at http://math.ut.ee/~toomas_l/harmonic_analysis/Fourier/F.html (2004/06/30).
- [9] Serabyn, Eugene: Nulling Interferometry and Planet Detection. *Course Notes from the 1999 Michelson Summer School*, August 1999.
- [10] Quirrenbach, Andreas: Observing Through the Turbulent Atmosphere. *Course Notes from the 1999 Michelson Summer School*, August 1999.
- [11] The XMM Satellite Schoolpage. *Why is diffraction so important?* Available at <http://www.sr.bham.ac.uk/xmm/diffpage2.html> (2004/07/13).